ChemComm

Accepted Manuscript

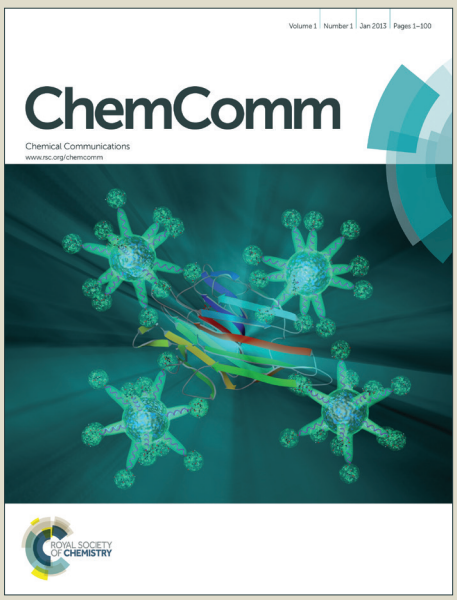

ROYAL SOCIETY OF CHEMISTRY

www.rsc.org/chemcomm

Journal Name

RSCPublishing

COMMUNICATION

Stability, durability and regeneration ability of a novel Ag-based photocatalyst $Ag_2Nb_4O_{11}$

Cite this: DOI: 10.1039/x0xx00000x

Hongjun Dong,[a, b] Gang Chen,*[a] Jingxue Sun, [a] Yujie Feng,*[c] Chunmei Li, [a] and Chade Lv [a]

Received 00th January 2014,
Accepted 00th January 2014

DOI: 10.1039/x0xx00000x

www.rsc.org/

A novel Ag-based photocatalyst $Ag_2Nb_4O_{11}$ is firstly obtained, which exhibits the universal high-efficiency photodegradation activity for RhB, MB and MO organic dyes. The persistent cycle reaction of 40 times and recovery characteristic indicate the $Ag_2Nb_4O_{11}$ photocatalyst has high stability, durability and regenerated ability.

Developing high-efficient semiconductor photocatalytic materials for eliminating organic contaminants in purification of environments has been considered to be an important field in the photocatalysis researches.[1] In recent years, Ag-based compounds as photocatalysts have been widely researched and believed to be a kind of promising photocatalytic materials,[2] which usually exhibit the high-efficiency photocatalytic oxidation ability for liberating O_2 from the water and degrading organic pollutants. One of the most important reasons is that the unique filled d^{10} electronic configuration of Ag^+ ions can take part in composition and hybridization of energy band structure.[3] A representative is a series of AgX (silver halide)[4] and Ag/AgX SPR (Surface Plasma Resonance) photocatalysts prepared by *in-situ* growth of silver nanoparticles on the silver halide surfaces.[5] Another one is Ag-based composite oxide photocatalysts. Especially, Ag_3PO_4 reported by J. H. Ye and co-workers displays the high-performance oxygen liberation ability from the water and photodegradation activity for organic dyes.[6] Up to now, the majority of experimental and theoretical works have been carried out to improve the photocatalytic activity of AgX and Ag_3PO_4 photocatalysts by using various techniques, such as manipulating morphology,[7] controlling lattice plane,[8] building hierarchical structure,[9] constructing heterojunction[10] and so forth. Nevertheless, these materials are so sensitive to light that they can take place photocorrosion unavoidable, which result in the shortening of operating life and reduction of photocatalytic activity. In addition, some other p- and d-block composite oxides containing Ag have been developed,[11] in which the most works usually concentrate on improving photocatalytic activity, controlling morphology and designing band gap engineering. However, it is regretful that the requisite durability, stability and regeneration ability are rarely considered, which are significant for photocatalyst to meet the requirement of recycling use in practical application. As far as the Ag-based compounds are concerned, possessing the high photocatalytic activity, long-term durability and regenerated ability are still a tremendous and difficult challenge.

At present work, a novel Ag-based photocatalyst $Ag_2Nb_4O_{11}$ is firstly achieved, which can degrade RhB, MB and MO organic dyes under UV-visible light. Interestingly, it has not obvious inactivation throughout the circle operations of 40 times enduring 1400 min reaction, which demonstrates that the merely slight photocorrosion has a little influence on the photocatalytic activity. The encouraging result is that the regeneration of $Ag_2Nb_4O_{11}$ is achieved by a simple re-calcination process and the degradation activity of palingenetic $Ag_2Nb_4O_{11}$ almost reaches to the primal level of the fresh sample.

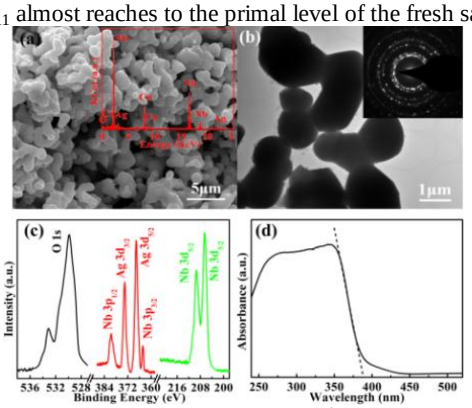

Fig. 1 SEM images (a), EDS spectra (the insert of a), TEM image (b), SAED pattern (the insert of b), XPS spectra (c) and UV-vis spectrum (d) of $Ag_2Nb_4O_{11}$ sample.

The SEM image (Fig. 1a) exhibits that the sample has irregular bulk distribution morphology and the EDS spectrum (the insert of Fig. 1a) indicates that the sample is composed of Ag, Nb and O elements. The TEM image (Fig. 1b) further revels that these bulks are aggregated by particles with size about 1-3 μm, which is attributed to the high-temperature calcination. The SAED pattern (the insert of Fig. 1b) performed on the whole bulk shows the bright diffraction rings, which indicates that the sample presents a polycrystalline characteristic.

The survey XPS spectrum (Fig. S1, ESI†) displays that the sample is composed of Ag, Nb and O elements in line with the EDS spectrum. From the XPS spectra of sample in Fig. 1c, two binding energy peaks at 529.9 and 533.1 eV indicate that oxygen has two

different chemical states[12] which derive from lattice O^{2-} 1s state of $Ag_2Nb_4O_{11}$ and adsorbed hydroxyl species,[13] respectively. In addition, the binding energy peaks of Ag $3d_{5/2}$ (367.7 eV) and Ag $3d_{3/2}$ (373.6 eV) can be assign to the Ag^+ chemical state.[14] The no-broadening and symmetric shape indicates that silver may only possesses one Ag^+ chemical state. Moreover, the XPS spectrum of Nb coincides with $3d_{3/2}$ and $3d_{5/2}$ states at 209.4 and 206.6 eV, in which the spin-orbit separation of 2.8 eV implies that Nb^{5+} ions exist in the sample.[14] In addition, the peaks at 364.2 and 380.5 eV ascribe to the Nb^{5+} $3p_{3/2}$ and $3p_{1/2}$ states,[14] respectively. The surface atomic ratio approximates to stoichiometric proportion (2:4:11) (Table S1, ESI†), which indicates that the pure $Ag_2Nb_4O_{11}$ product is obtained.

The UV-visible DRS spectrum of sample (Fig. 1d) presents a strong absorption within 387 nm. The steep shape indicates that the absorption is due to the intrinsic band gap transition of sample rather than impurity levels. The band edge and semiconductor type of $Ag_2Nb_4O_{11}$ are estimated with empirical equations of the crystal semiconductor (Fig. S2, ESI†). The results indicate that $Ag_2Nb_4O_{11}$ exhibits the indirect band gap of 3.09 eV as well as direct transition of 3.30 eV, respectively.[6] The narrower band gap of $Ag_2Nb_4O_{11}$ than that of Nb_2O_5 (3.4 eV)[15] implies the easy exciting electrons from the VB to CB to improve photocatalytic activity. It arises from that Ag^+ ions introduced into Nb_2O_5 participate in construction of the new crystal structure and energy band structure.

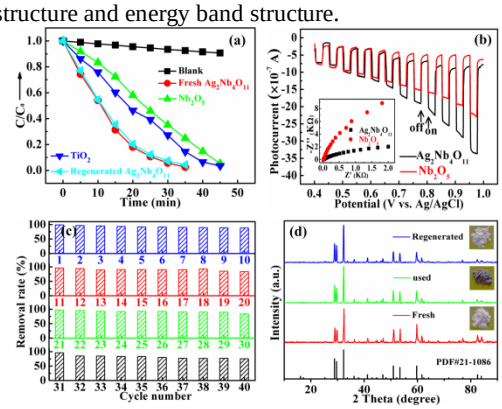

Fig. 2 Dynamic curves of RhB solutions over different sample (a), photocurrent responses (b) and EIS spectra (the insert of b) of $Ag_2Nb_4O_{11}$ and Nb_2O_5 as electrodes, circle operation of the RhB solution degradation (c), XRD pattern and color of the fresh, used and regenerated $Ag_2Nb_4O_{11}$ samples (d).

The dynamic curves of RhB solution degradation (Fig. 2a) show that RhB is completely degraded over $Ag_2Nb_4O_{11}$ within 35 min which is less than that of Nb_2O_5 and TiO_2. No-shifting and vanishing of the absorption peaks of RhB solutions from ultraviolet to visible region (Fig. S3, ESI†) prove that the benzene/heterocyclic rings of RhB molecule are decomposed into small organic/inorganic molecules or/and ions products.[16] Even if MB and relatively stable MO azo dye are serve as target molecules, the removal rates can also exceed 96% and 80% after 25 and 90 min, respectively (Fig. S4-S5, ESI†). The above results indicate that the photocatalytic activity of $Ag_2Nb_4O_{11}$ photocatalyst is conspicuous superior to that of Nb_2O_5 and TiO_2, and exhibits universality for degradation of various organic dyes.

The photocatalytic reaction can be further regarded as a photoelectrochemical process.[17] The positive slope of Mott-Schottky plots of $Ag_2Nb_4O_{11}$ and Nb_2O_5 electrodes (Fig. S6, ESI†) indicates that they are n-type semiconductor. The flat-band potential of $Ag_2Nb_4O_{11}$ (-0.72 V) is higher than that of Nb_2O_5 (-0.62 V). Therefore, the CB of $Ag_2Nb_4O_{11}$ is more negative because the CB is approach to flat-band potential in n-type semiconductors,[18] which is consistent with the calculated results using empirical formulae (Table S2, ESI†). It means that $Ag_2Nb_4O_{11}$ has the more intense reducing capacity in favour of capturing H_2O_2 molecules to yield hydroxyl radical (•OH) decomposing dyes. Moreover, The $Ag_2Nb_4O_{11}$ electrode presents a more intense photocurrent response than Nb_2O_5 electrode (Fig. 2b), which evidences the more effective separation of carriers and faster charge transfer through $Ag_2Nb_4O_{11}$ electrode interface.[19] The result is further proved by EIS (Electrochemical Impedance Spectra) of them (the insert of Fig. 2b). The arc radius on the Nyquist plot of $Ag_2Nb_4O_{11}$ electrode is smaller than that of Nb_2O_5 electrode, which implies that the former has better high-efficiency charge transfer ability. Therefore, the improved separation and transfer efficiency of carriers may be main reason for the high degradation activity of $Ag_2Nb_4O_{11}$.[17] In addition, the large BET specific surface area of $Ag_2Nb_4O_{11}$ (4.582 m^2 g^{-1}) relative to Nb_2O_5 (1.997 m^2 g^{-1}) is also play a role for improving degradation activity.

Furthermore, the circle operation of degrading RhB is performed (Fig. 2c). The photocatalytic ability of $Ag_2Nb_4O_{11}$ sample has not obviously loss after 40 recycles enduring 1400 min reaction. The removal rate still achieves 75% within 35 min in the last 40th circle. Meanwhile, the XRD pattern (Fig. 2d) shows that the fresh sample is well-indexed as hexagonal $Ag_2Nb_4O_{11}$ (PDF#21-1086). The sharp diffraction peaks imply the pure sample with high-crystallinity is achieved. After circle operation of 40 times, the color of sample changing white into dark grey suggests that Ag nanoparticles generates on the $Ag_2Nb_4O_{11}$ surface under light irradiation, which is similar to most Ag-based photocatalysts. It is worth noting that the XRD pattern of the used sample (Fig. 2d) is nearly unchanged, and in which no Ag phase is detected. It indicates that $Ag_2Nb_4O_{11}$ is a relatively stable Ag-based photocatalyst with slight photocorrosion. Moreover, when the used sample is performed by a re-calcination process, the dark grey changes into white again and the XRD pattern (Fig. 2d) still displays the pure $Ag_2Nb_4O_{11}$ phase as well as XPS spectra peaks of elements are almost same as that of the fresh sample (Fig. S7 ESI†). It demonstrates that the $Ag_2Nb_4O_{11}$ photocatalyst realizes regeneration. More importantly, the degradation ability of regenerated sample almost reaches to the primal level of the fresh sample (Fig. 2a). It indicates that $Ag_2Nb_4O_{11}$ as a novel Ag-based photocatalyst possesses the splendid stability, durability and regeneration ability.

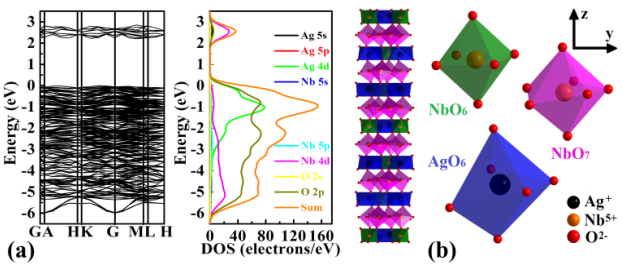

Fig. 3 Energy band diagram and DOS (a), crystal structure of $Ag_2Nb_4O_{11}$ (b).

The activity and stability of photocatalyst are determined by its electronic structure and crystal structure in essence. The theoretical calculation are performed based on *ab* initio density functional theory (ESI†). The calculated electronic band structure diagram of $Ag_2Nb_4O_{11}$ (Fig. 3a) confirms its indirect transition characteristic. The relative flatness of CB bottom and VB top implies that it also yields a direct transition under a little high energy, which agrees well with the result revealed by UV-vis DRS. Density of States (DOS) of $Ag_2Nb_4O_{11}$ indicates that VB top of $Ag_2Nb_4O_{11}$ is mainly composed of the hybridized Ag 4d and O 2p orbital, which leads to the VB top of $Ag_2Nb_4O_{11}$ shifting up relative to that of Nb_2O_5 composed by only O 2p orbital. It brings about narrowing band gap and enhancing light harvest ability to improve photocatalytic activity. This hybridized

effect has also been reported in the most Ag-based photocatalysts.[3] In addition, the high degree of overlap indicates that the intense bonding effect exists in Ag 4d and O 2p orbital, which contribute significantly to improving stability of $Ag_2Ta_4O_{11}$. The CB bottom of $Ag_2Nb_4O_{11}$ is mainly composed of Nb 4d orbital and accompanied a little O 2p and Ag 5s states. Because the mobility of charge carriers is proportional to the reciprocal their effective mass, the little Ag 5s state in the CB can reduce electron effective mass and increase delocalization, thus also improving photocatalytic ability.[3b]

$Ag_2Nb_4O_{11}$ is a typical layered structure niobate, which belongs to a member of family compounds with general formula $A_xNb_{3n+1}O_{8n+3}$ (n = 1).[20] As shown in Fig. 3b, the linked alternately NbO_6 and AgO_6 octahedrons as well as NbO_7 pentagonal bipyramids construct a polyhedron layer in X-Y plane, respectively. Two polyhedron layers alternately stack along Z-axis by corner-connecting to build the three-dimensional framework. Most layer-structured compounds have been previously developed as efficient photocatalysts because the layered structure can improve the separation and transportation of charge carriers.[21] In the $Ag_2Nb_4O_{11}$ crystal, the interlaced network of AgO_6 and NbO_6 octahedrons in one layer of X-Y plane is beneficial to separation and migration of charge carriers from the hybridized Ag 4d and O 2p orbitals to the unoccupied Nb 4d orbitals. Especially, it is similar to tantalate[22] that the bond angle of Nb-O-Nb is equal to 180 ° in NbO_6, so the photogenerated charge carriers can migrate easily in the framework of NbO_6 units. In addition, the bond angle of O-Nb-O reaches to 135.6 ° between NbO_6 and NbO_7, which facilitates electron transfer in two layers. The NbO_7 layers can serve as electron transportation channel to improve the transfer and separation efficiency of electron-hole pairs.[3d] Moreover, the formation of AgO_6 octahedrons is crucial to the stability of $Ag_2Nb_4O_{11}$, where the central Ag^+ ion is encircled by surrounding six O^{2-} ions that plays a protection role *via* forming intense coordinate bond. It restrains efficiently Ag^+ ions dissociate from $Ag_2Nb_4O_{11}$ crystal and avoid being reduced by photogenerated electrons. Meanwhile, the same layered NbO_6 and the near layered NbO_7 connecting with AgO_6 can rapidly export photogenerated electrons generated in AgO_6, which separates charge carriers and inhibits the reduction of Ag^+ ions in the crystal structure.

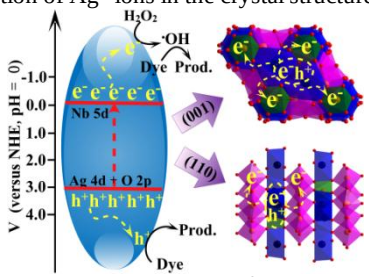

Scheme 1 Transferred and separated behavior of charge carriers in the crystal along to (001) and (110) crystal lattice plane view and photocatalytic reaction mechanism of dye over the $Ag_2Nb_4O_{11}$ sample.

Scheme 1 illustrates the transfer and separation behavior of the charge carriers in the $Ag_2Nb_4O_{11}$ crystal along to (001) and (110) crystal lattice plane view and photocatalytic reaction mechanism. When $Ag_2Nb_4O_{11}$ sample is exposed to the UV-visible light, the electron-hole pairs are produced on AgO_6 octahedrons. At the same time, the electrons transfer to the dominant Nb 4d orbital at the CB bottom, and the holes transfer to the hybridized Ag 4d and O 2p orbital at the VB top. In consequence, the electron transport channels are formed in NbO_6 and NbO_7 as well as the hole transport channels are formed in AgO_6, respectively. Finally, the electrons and holes migrate to the sample surface through electron and hole transport channels, respectively. Electrons further are captured by H_2O_2 in the solution to generate ·OH activated species to decompose dyes. Holes can also directly decompose dyes.

In summary, a novel Ag-based photocatalyst $Ag_2Nb_4O_{11}$ is firstly obtained, which exhibits universal degradation ability for RhB, MB and MO organic dyes under UV-visible light, as well as excellent stability, durability and regeneration ability. Photoelectrochemical characteristics reveal that the enhanced reducing capacity as a result of shifting up of CB and improved separation efficiency of charge carriers are mainly reason of the high degradation activity. The unique electronic structure and crystal structure determine its high photocatalytic activity and stability in essence. This work exploits a stable and renewable Ag-based photocatalyst, which makes an important step for the development of Ag-based photocatalyst.

This work was financially supported by the National Nature Science Foundation of China (21071036 and 21271055) and Province Natural Science Foundation of Heilongjiang Province (ZD201011). We acknowledge for the support by Open Project of State Key Laboratory of Urban Water Resource and Environmen, Harbin Institute of Technology (No. QAK201304) and Program for Innovation Research of Science in Harbin Institute of Technology.

Notes and reference

a Department of Chemistry, Harbin Institute of Technology, Harbin 150001, P. R. China.
b Department of Chemistry, Baicheng Normal University, Baicheng 137000, P. R. China.
c State Key Laboratory of Urban Water Resource and Environment, Harbin Institute of Technology, Harbin 150090, P. R. China.

† Electronic Supplementary Information (ESI) available: Experimental details and additional fgures and table. See DOI: 10.1039/b000000x/

1 C. Chen, W. Ma and J. Zhao, *Chem. Soc. Rev.*, 2010, **39**, 4206-4219.

2 (*a*) H. Tong, S. Ouyang, Y. Bi, N. Umezawa, M. Oshikiri and J. Ye, *Adv. Mater.*, 2012, **24**, 229-251. (*b*) P. Wang, B. Huang, Y. Dai and M. H. Whangbo, *Phys. Chem. Chem. Phys.*, 2012, **14**, 9813-9825.

3 (*a*) S. Ouyang and J. Ye, *J. Am. Chem. Soc.*, 2011, **133**, 7757-7763; (*b*) H. Shi, Z. Li, J. Kou, J. Ye and Z. Zou, *J. Phys. Chem. C*, 2011, **115**, 145-151; (*c*) N. Umezawa, S. Ouyang and J. Ye, *Physical Review B*, 2011, **83**, 035202-035208; (*d*) J. Boltersdorf, T. Wong and P. A. Maggard, *ACS Catal.*, 2013, **3**, 2943-2953; (*e*) M. Li, J. Zhang, W. Dang, S. K. Cushing, D. Guo, N. Wu and P. Yin, *Phys. Chem. Chem. Phys.*, 2013, **15**, 16220-16226.

4 (*a*) Z. Lou, B. Huang, Z. Wang, X. Qin, X. Zhang, Y. Liu, R. Zhang, Y. Dai and M. H. Whangbo, *Dalton Trans.*, 2013, **42**, 15219-15225; (*b*) Z. Lou, B. Huang, X. Ma, X. Zhang, X. Qin, Z. Wang, Y. Dai and Y. Liu, *Chem. Eur. J.*, 2012, **18**, 16090-16096; (*c*) H. Wang, J. Gao, T. Guo, R. Wang, L. Guo, Y. Liu and J. Li, *Chem. Commun.*, 2012, **48**, 275-277; (*d*) W. Jiang, C. An, J. Liu, S. Wang, L. Zhao, W. Guo and J. Liu, *Dalton Trans.*, 2014, **43**, 300-305.

5 (*a*) Y. Tang, Z. Jiang, G. Xing, A. Li, P. D. Kanhere, Y. Zhang, T. C. Sum, S. Li, X. Chen, Z. Dong and Z. Chen, *Adv. Funct. Mater.*, 2013, **23**, 2932-2940; (*b*) L. Han, Z. Xu, P. Wang and S. Dong, *Chem. Commun.*, 2013, **49**, 4953-4955; (*c*) K. Dai, L. Lu, J. Dong, Z. Ji, G. Zhu, Q. Liu, Z. Liu, Y. Zhang, D. Li and C. Liang, *Dalton Trans.*, 2013, **42**, 4657-4662; (*d*) C. Hu, T. Peng, X. Hu, Y. Nie, X. Zhou, J. Qu and H. He, *J. Am. Chem. Soc.*, 2010, **132**, 857-862.

6 Z. Yi, J. Ye, N. Kikugawa, T. Kako, S. Ouyang, H. Stuart-Williams, H. Yang, J. Cao, W. Luo, Z. Li, Y. Liu and R. L. Withers, *Nat. Mater.*, 2010, **9**, 559-563.

7 (*a*) R. Dong, B. Tian, C. Zeng, T. Li, T. Wang and J. Zhang, *J. Phys. Chem. C*, 2013, **117**, 213-220; (*b*) M. Zhu, P. Chen and M. Liu, *Langmuir*, 2013, **29**, 9259-9268; (*c*) C. An, S. Peng and Y. Sun, *Adv. Mater.*, 2010, **22**, 2570-2574; (*d*) D. Chen, S. H. Yoo, Q. Huang, G. Ali and S. O. Cho, *Chem. Eur. J.*, 2012, **18**, 5192-5200; (*e*) H. Hu, Z. Jiao, H. Yu, G. Lu, J. Ye and Y. Bi, *J. Mater. Chem. A*, 2013, **1**, 2387-2390; (*f*) Y. S, Xu and W. D. Zhang, *CrystEngComm*, 2013, **15**, 5407-5411; (*g*) H. Hu, Z. Jiao, T. Wang, J. Ye, G. Lu and Y. Bi, *J. Mater. Chem. A*, 2013, **1**, 10612-10616.

8 (*a*) Z. Lou, B. Huang, X. Qin, X. Zhang, H. Cheng, Y. Liu, S. Wang, J. Wang and Y. Dai, *Chem. Commun.*, 2012, **48**, 3488-3490; (*b*) Z. Jiao, Y. Zhang, H. Yu, G. Lu, J. Ye and Y. Bi, *Chem. Commun.*, 2013, **49**, 636-638; (*c*) Z. Lou, B. Huang, Z. Wang, R. Zhang, Y. Yang, X. Qin, X. Zhang and Y. Dai, *CrystEngComm*, 2013, **15**, 5070-5075; (*d*) D. J. Martin, N. Umezawa, X. Chen, J. Ye and J. Tang, *Energy Environ. Sci.*, 2013, **6**, 3380-3386; (*e*) J. Wang, F. Teng, M. Chen, J. Xu, Y. Song and X. Zhou, *CrystEngComm*, 2013, **15**, 39-42; (*f*) B. Zheng, X. Wang, C. Liu, K. Tan, Z. Xie and L. Zheng, *J. Mater. Chem. A*, 2013, **1**, 12635-12640.

9 (*a*) P. Wang, B. Huang, Z. Lou, X. Zhang, X. Qin, Y. Dai, Z. Zheng and X. Wang, *Chem. Eur. J.*, 2010, **16**, 538-544; (*b*) J. D. Wang, J. K. Liu, C. X. Luo, Y. Lu and X. H. Yang, *Cryst. Growth Des.*, 2013, **13**, 4837-4843.

10 (*a*) G. Luo, X. Jiang, M. Li, Q. Shen, L. Zhang and H. Yu, *ACS Appl. Mater. Interfaces*, 2013, **5**, 2161-2168; (*b*) D. Wang, Y Li, G. L. Puma, C. Wang, P. Wang, W. Zhang and Q. Wang, *Chem. Commun.*, 2013, **49**, 10367-10369; (*c*) P. Wang, Y. Tang, Z. Dong, Z. Chen and T. T. Lim, *J. Mater. Chem. A*, 2013, **1**, 4718-4727; (*d*) Y. G. Lin, Y. K. Hsu, Y. C. Chen, S. B. Wang, J. T. Miller, L. C. Chen and K. H. Chen, *Energy Environ. Sci.*, 2012, **5**, 8917-8922; (*e*) C. An, W. Jiang, J. Wang, S. Wang, Z. Ma and Y. Li, *Dalton Trans.*, 2013, **42**, 8796-8801.

11 (*a*) T. Kako, N. Kikugawa and J. Ye, *Catal. Today*, 2008, **131**, 197-202; (*b*) H. Kato, H. Kobayashi and A. Kudo, *J. Phys. Chem. B*, 2002, **106**, 12441-12447; (*c*) S. Ouyang, N. Kikugawa, D. Chen, Z. Zou and J. Ye, *J. Phys. Chem. C*, 2009, **113**, 1560-1566; (*d*) S. Wang, D. Li, C. Sun, S. Yang, Y. Guan and H. He, *Appl. Catal. B: Environ.*, 2014, **144**, 885-892; (*e*) G. Li, Y. Bai, W. F. Zhang and H. Zhang, *Mater. Chem. Phys.*, 2013, **139**, 1009-1013; (*f*) K. Saito, S. Kazama, K. Matsubara, T. Yui and M. Yagi, *Inorg. Chem.*, 2013, **52**, 8297-8299; (*g*) S. Song, Y. Zhang, Y. Xing, C. Wang, J. Feng, W. Shi, G. Zheng and H. Zhang, *Adv. Funct. Mater.*, 2008, **18**, 2328-2334; (*h*) J. Tang, Y. Liu, H. Li, Z. Tan and D. Li, *Chem. Commun.*, 2013, **49**, 5498-5500.

12 M. T. Uddin, Y. Nicolas, C. Olivier, T. Toupance, L. Servant, M. M. Müller, H. J. Kleebe, J. Ziegler and W. Jaegermann, *Inorg. Chem.*, 2012, **51**, 7764-7773.

13 J. B. Mu, C. L. Shao, Z. C. Guo, Z. Y. Zhang, M. Y. Zhang, P. Zhang, B. Chen and Y. C. Liu, *ACS Appl. Mater. Interfaces*, 2011, **3**, 590-596.

14 W. Wu, S. Liang, Y. Chen, L. Shen, R. Yuan, and L. Wu, *Mater. Res. Bull.*, 2013, **48**, 1618-1626.

15 Y. Zhao, X. Zhou, L. Ye and S. C. E. Tsang, *Nano Reviews*, 2012, **3**, 17631-17642.

16 H. J. Dong, G. Chen, J. X. Sun, C. M. Li, Y. G. Yu and D. H. Chen, *Appl. Catal. B: Environ.*, 2013, **134-135**, 46-54.

17 (a) Z. H. Zhang, R. Dua, L. B. Zhang, H. B. Zhu, H. G. Zhang and P. Wang, *ACS Nano.*, 2013, **7**, 1709-1717; (b) Q. W. Huang, S. Q. Tian, D. W. Zeng, X. X. Wang, W. L. Song, Y. Y. Li, W. Xiao and C. S. Xie, *ACS Catal.*, 2013, **3**, 1477-1485.

18 Y. H. Ng, I. V. Lightcap, K. Goodwin, M. Matsumura and P. V. Kamat, *J. Phys. Chem. Lett.*, 2010, **1**, 2222-2227.

19 M. Sun, G. D. Chen, Y. K. Zhang, Q. Wei, Z. M. Ma and B. Du, *Ind. Eng. Chem. Res.*, 2012, **51**, 2897-2903.

20 N. Masó, D. I. Woodward, P. A. Thomas, A. Várez and A. R. West, *J. Mater. Chem.*, 2011, **21**, 2715-2722.

21 M. Guan, C. Xiao, J. Zhang, S. Fan, R. An, Q. Cheng, J. Xie, M. Zhou, B. Ye and Y. Xie, *J. Am. Chem. Soc.*, 2013, **135**, 10411-10417.

22 T. Xu, X. Zhao and Y. Zhu, *J. Phys. Chem. B*, 2006, **110**, 25825-25832.

